Triple product acousto-optical processor for the astrophysical applications

Principle contributors:

Alexandre S. Shcherbakov [(1)], Ana Virginia Hanessian de la Garza [(1)], Vahram Chavushyan [(1)], and Joaquin Campos Acosta [(2)].

1) National Institute for Astrophysics, Optics, and Electronics (INAOE), Puebla, 72000, Mexico.

2) CSIC – Institute for Applied Physics, Madrid, 28006, Spain.

National Institute for Astrophysics, Optics, and Electronics (INAOE),

Puebla, Mexico.

Department for Optics, INAOE

Technical report

INDEX

ABSTRACT

Both a high level of developing the spatially spot-like and one-dimensional input devices and the flexibility of a design inherent in two-dimensional optical systems with similar modulating components make it possible to realize various opto-electronic processing systems with an improved productivity. This is why a one-dimension acousto-optic technique can be successfully involved into developing an extremely high-bit-rate data processor based on the algorithm of triple product correlations. Practically, triple product correlations originate within an optical scheme including the modulated light source, representing the first input port, and two wide-aperture acousto-optical cells forming two other input ports. Due to specifically constructed lens system, initially modulated light beam is crossing sequentially the apertures of acousto-optical cells oriented at right angle to each other. Finally, a CCD-matrix integrates the received optical signal with respect to time and registers the resulting triple product correlations. In a view of arranging similar acousto-optical processor for modeling triple product correlations, potential performances of the progressed design for similar processor are estimated as well.

This triple product acousto-optical processor is oriented to studies in the extra-galactic astronomy as well as to searching the extra-solar planets, so that algorithm of the space-and-time integrating is desirable for a wideband spectrum analysis with an improved resolution. It includes $\mathbf{1D}$-acousto-optic cells as the input devices for a $\mathbf{2D}$-optical data processing. The importance of this algorithm is based on exploiting the chirp $\mathbf{Z}-$transform technique providing a $\mathbf{2D}$-Fourier transform of the input signals. The system produces the folded spectrum, accumulating advantages of both space and time integrating. Its frequency bandwidth is practically equal to the bandwidth of transducers inherent in acousto-optical cells. Then, similar processor is able to provide really high frequency resolution, which is practically equal to the reciprocal of the CCD-matrix photo-detector integration time. Here, the current state of designing the triple product acousto-optical processor in frames of the astrophysical instrumentation is presented.

Key words: acousto-optics, data processing, triple product processor, space-and-time integrating, schematic arrangement, astrophysical instrumentation.

1. INTRODUCTION: A TWO-DIMENSIONAL SIGNAL PROCESSING BASED ON SPATIALLY ONE-DIMENSIONAL INPUT DEVICES

Spectrum analysis is the most widely used in physical sciences technique for obtaining the information about unknown signals. In so doing, the Fourier transform algorithm, which appears perfectly naturally in optical systems with coherent lighting, plays the central role in spectrum analysis. Periodical signals produce the light scattering in rather definite directions that can be found easily in the Fourier domain in comparison with space or time domains, because the energy of each individual frequency component is concentrated in a particular point on the Fourier plane. Consequently, the matrix of photo-detectors, placed into the Fourier plane, will be able to detect a spectrum and to convert it into electronic signal for the following processing. The main expected advantage from creating optical Fourier-processors is the ability of a thin lens to produce a $\mathbf{2D-}$ Fourier transform of an input signal, which that signal should be highly coherent as, for instance, laser radiation. In this case, the calculation of a $\mathbf{2D-}$ Fourier transform performs completely parallel for various points "just literally" with the light velocity ($\mathbf{0.3\,m/ns}$). It is equivalent to the bit-rate about $\mathbf{4\cdot 10^{15}}$ mathematical operations per second for the $\mathbf{2D-}$ data massive of $\mathbf{256\times 256}$ pixels in optical system of $\mathbf{30\,cm}$ in length exploiting about $\mathbf{20\,mW}$ laser source. In fact, this estimation is based on a number of multiplication and summarizing operations needed for carrying out the corresponding electronic procedure within the well-known Fast-Fourier-Transform algorithm. Just this estimation for the speed of operations inherent in optical data processing supported and supports now the practical interest in designing similar systems.

One can consider a one-dimensional analyzer for the instant spectrum of power. Within this device, every moment of time the Fourier transform is calculating only for a part of a signal, which is currently placed inside of an acousto-optical cell. Due to similar calculations will be finished as soon as light will have passed through a plane of the Fourier transform, one can consider these calculations like instantly performed ones. Then, the word "power" means that the matrix of photo-detectors is able to separate only the intensity of light, and this light intensity is directly proportional to a portion of the ultra-high-frequency radio-wave power in the input electronic signal. Optical spectrum analyzers can be divided into a pair of really large groups depending on the variable chosen for the Fourier transform. In fact, there are two options: to chose space or time variable for the following transform. Of course, one can combine them to realize a hybrid system for spectrum analysis.

Generally, the systems for optical information processing have an advantage to be a three-dimensional in their nature, so that the directions of propagating the corresponding light flows can be usually considered as optical axes. During the propagation of light through each of similar systems the modulations of light flow by the input data and the other optical transformations can be performed to obtain the desirable issuing light distribution at the output plane of that system. Usually, various modulators, lenses, and other components for optical data processing are located in the planes being orthogonal to optical axis, so that a two-dimension arrangement makes it possible to carry out a large amount of parallel operations and, in so doing, to realize potentially ultra-high productivity of computations. Together with this, during the last years a lot of two-dimensional architectures for optical data processing has been progressed, wherein various one-dimensional input devices have been exploited, while the these systems as a whole have been designed in a

three-dimension space. Realizing two-dimensional optical processors with one-dimensional input devices is not so easy, as a rule; nevertheless, similar systems exhibit a high level of flexibility. As a result, rather large amount of high-quality one-dimensional input devices has been created and inserted into optical systems for two-dimensional data processing in a view of creating high-bit-rate and adaptable optical processors. One of the most important arguments for applying one-dimensional input devices in two-dimensional processing is based on relatively high level of their development. The most wide-spread of them are, for example, linear arrays of semiconductor light sources like laser diodes or light emission diodes (LEDs); then, one can call a row of electro-optic, acousto-optic, and magneto-optic cells; various CCD linear arrays, etc. It should be noted that modern semiconductor light sources allow effective and ultra-high frequency (up to $\mathbf{10^{10}}$ **Hz**) external amplitude modulation, while one-dimensional Bragg acousto-optical cells (AOCs) provide effective conversion of electrical signal into optical ones in a wide (up to a few gigahertz) frequency bandwidth with time-bandwidth product (i.e. a product of the frequency bandwidth and the aperture transit time) exceeding $\mathbf{10^3}$. Rather small sizes of similar input devices and modern technique of designing the needed optical lenses give real opportunity for constructing ultra-high-productive and compact optical systems for parallel data processing. Moreover, both relatively low levels of the needed electric power and not high prices inherent in these components lead potentially to realizing compact optical processors of low power consumption as well as of low cost.

2. A TRIPLE-PRODUCT ACOUSTO-OPTICAL PROCESSOR

In this article, an extremely adaptable optical architecture of an acousto-optical triple-product processor, which had been initially suggested in Ref.[2.1, 2.2] and whose general schematic arrangement is presented in Fig.2.1, will be discussed.

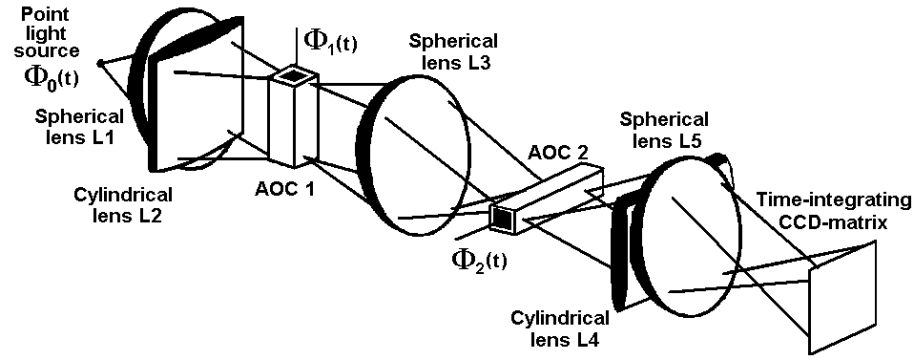

a. General schematic arrangement of optical components.

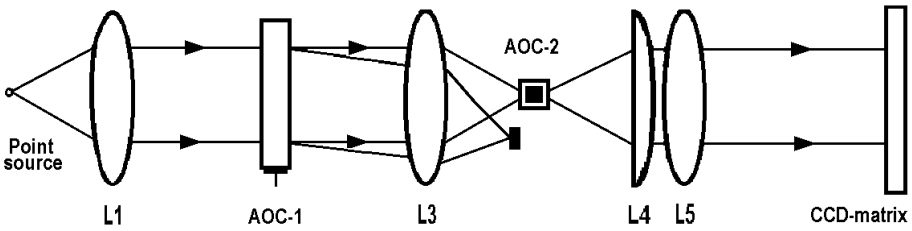

b. Front view.

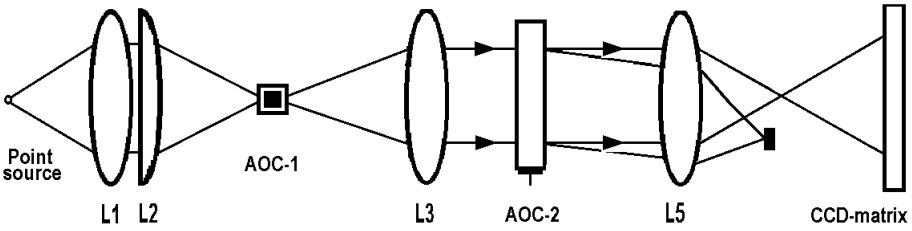

c. Top view.

Figure 2.1. Schematic arrangement for a triple-product acousto-optical processor.

The laser diode or LED, for example, can be used as a point light source whose radiation is modulated in time by the initial electronic signal $\Phi_0(t)$. The vertically oriented acousto-optic cell AOC-1 realizes a modulation by the first additional electronic signal $\Phi_1(t)$. This cell is lighted by the optical beam from a point source through the spherical lens $L1$ and the cylindrical lens $L2$. The light beam, scattered by the AOC-1, is modulated by the product $\Phi_0(t)\cdot\Phi_1(t-x_1/V_1)$. In a view of lighting the AOC-2, which is placed horizontally, the output light beam after the AOC-1 is

broadened horizontally and focused vertically by the spherical lens $\mathbf{L3}$. Let the second additional electronic signal, which is applied to the AOC-2, is $\Phi_2(t)$. As a result, the light beam, scattered by the AOC-1, is modulated by the product $\Phi_0(t)\cdot\Phi_1(t-x_1/V_1)\cdot\Phi_2(t-x_2/V_2)$. The obtained product includes in fact two time delays $t_1 = x_1/V_1$ and $t_2 = x_2/V_2$, where $x_{1,2}$ and $V_{1,2}$ are physical spatial coordinates along the corresponding acousto-optical cells and the acoustic wave velocities, respectively. These time delays t_1 and t_2 must satisfy the inequality $0 < (t_1, t_2) < T$, where the aperture transit time T of the modern acousto-optical cells can be equal to about $10-50\,\mu s$. The cylindrical lens $\mathbf{L4}$ and the spherical lens $\mathbf{L5}$ shape the image of the AOC-2 at the output plane in horizontal direction, while the spherical lenses $\mathbf{L3}$ and $\mathbf{L5}$ give the image of the AOC-1 at the output plane in vertical direction. A two-dimensional matrix of photo-detectors is placed in the output plane, so that charges $g(t_1, t_2)$ collected by each individual pixel under acting the light during the time T_i at a point (x,t) are proportional to

$$g(t_1, t_2) = \int_{T_i} \Phi_0(t)\ \Phi_1(t - x_1/V_1)\ \Phi_2(t - x_2/V_2)\, dt, \qquad (2.1)$$

where T_i is the time of integration, which is limited by the detector and could be about $1\,ms$ or more; the time delays t_1 and t_2 represent a pair of the coordinates in the output focal plane, i.e. in a plane of the CCD matrix photo-detector. Such a system represents a triple-product processor. Two additional views, depicted in Figs.2b and 2c, show that this processor consists of a pair of the two one-dimensional correlators operating simultaneously in two mutually orthogonal planes. However, the system does not simply collect two one-dimensional conversions; the final result appears within a joint two-dimensional processing of all the input signals. This architecture always calculates Eq.(2.1), but it exhibits really high flexibility, because all the three input signals are given initially as electronic signals, so that this processor can be easily re-oriented from fulfilling one algorithm to another in the frames of completely the same optical resources simply by varying the input electronic signals $\Phi_j(t)$ with $(j = 0,1,2)$.

3. SPATIALLY ONE-DIMENSIONAL ACOUSTO-OPTICAL INPUT DEVICES

In the case of exploiting spatially one-dimensional AOC as an input device, the data can be introduced in a sequential regime. If the signal applied to similar AOC is modulated by the time function $f(t)$, the light scattered by this cell will be modulated by the function $f(t-x/V)$, where x is the coordinate of acoustic wave propagation and V is the acoustic wave velocity. Consequently, at each instant of time t the scattered light is modulated proportionally to the input electric signal with respect to the spatial coordinate x; and together with this light is modulated by the input electric signal at each individual value of the coordinate x with respect to the time t. Such a doubled modulation can be important within designing dynamic optical processors, because in the last case the AOC can be exploited as the input devices and as the delay lines. In reality, the modulation provided by AOC is much more complicated process. The scattered light has Doppler frequency shift relative to the initial central frequency, and finite size of the AOC's aperture always restricts the spatial length of an area wherein the modulation of light beam can be fulfilled. Then, the proportionality between the depth of light modulation and the applied electric signal is true only when diffraction efficiency of the AOC does not exceed a few percents. Additionally, the modulating properties of AOC operating in Bragg regime are essentially depending on the angle of light incidence on a cell. All these factors should be taken into account during the design of practical systems.

The AOC can be efficiently used as a point modulator as well, because it can provide pure amplitude modulation for the light beam entirely. Within such an application of the AOC, one can imagine that the AOC's aperture is going to zero, so that space-time signal $f(t-x/V)$ is degenerated into the time function $f(t)$. If, for example, the AOC is lighted by a conic optical beam focused near the piezo-electric transducer, the scattered optical beam represents almost the same cone modulated with respect to time by the function $f(t)$. The bandwidth of modulation is inversely-proportional to the acoustic transit time through an individual focal spot. For example, with the focal spot size of about $4\,\mu m$ and typical acoustic wave velocity $4\cdot 10^5\ cm/s$, the acoustic transit time through that focal spot has the order of $1\,ns$. It should be noted that with growing the Klein-Cook parameter [3.1], which is accompanied by increasing the diffraction efficiency of AOC, the output light cone assumes an elliptic shape due to appearing wave mismatch. Nevertheless, this estimation is rather close to allowable time of direct electronic amplitude modulation for the laser diodes or LEDs. However, sometimes these light sources exhibit the radiation with too low time coherence under action of high-bit-rate modulation. This is why just the AOCs can be efficiently exploited as point modulators providing a wideband time modulation of light beam as a whole.

Nevertheless, efficiency of exploiting the third dimension in a three-coordinate space has the decisive significance, because just this property gives potential advantages to optical systems in comparison with the other ones. Consequently, an important question appears: is a two-dimensional data processing system capable of providing rather high productivity under exploitation of just one-dimensional input devices? The adequate answer looks like this: if a one-dimensional input device is involved, some part of functional possibilities of parallel processing becomes to be lost, because instead of about 10^6 resolvable spots of data, provided usually by a spatially two-dimensional light modulator, now only 10^3 spots can be realized. However, the losses in parallelism can be

successfully compensated by very wide frequency bandwidth of already existing one-dimensional input devices. Let us consider a few estimations. The aperture transit time $\mathbf{T}$ of the AOC can be undoubtedly about $\mathbf{30\,\mu s}$ (see below) or even more up to $\mathbf{0.1\,ms}$. The frequency bandwidth $\mathbf{\Delta f}$ of similar AOC is usually about $\mathbf{50\,MHz}$ or more. Consequently, the time-bandwidth product can be definitely estimated as $\mathbf{N = T \cdot \Delta f \geq 10^3}$, which represents the number of potentially achievable resolvable spots. This product is almost independent on concrete magnitudes of both $\mathbf{T}$ and $\mathbf{\Delta f}$, because it is mainly conditioned by fundamental acousto-optical relations. The direct comparisons of different processors are not always possible, but some estimation can be done. For example, if the AOC with the product $\mathbf{N = T \cdot \Delta f}$ is lighted by the modulated beam from a single-channel source and the frequency bandwidth of this external modulation is taken equal to $\mathbf{\Delta f}$ as well, one yields $\mathbf{\Delta f \cdot N}$ of multiplications per second, because during each time interval $\mathbf{1/\Delta f}$ one can realize $\mathbf{N}$ multiplications. In the case, when a pair of similar AOC is located sequentially, the triple-product processor will perform $\mathbf{\Delta f \cdot N^2}$ multiplications per second. As a result, using the above-mentioned estimations for the aperture transit time and the frequency bandwidth for the AOC, one can expect the final bit-rate about $\mathbf{10^{14-15}}$ multiplications per second. Thus, one can conclude that involving one-dimensional input devices with really wide frequency bandwidth in two-dimensional optical systems provides potentially creating the prototypes of rather high-bit-rate optical processors.

4. GENERAL SCHEMES FOR THE SPACE INTEGRATION AND THE TIME INTEGRATION SPECTRUM ANALYZERS

4.1. BASIC SPECTRUM ANALYZER WITH THE SPACE INTEGRATION

One of the ways for electronic spectrum analysis of a radio-wave signal consists in scanning the frequency range of interest sequentially using the super heterodyne receiver. In so doing, the receiver measures the energy in a narrow band near the central frequency. If the goal is to increase the sensitivity of that receiver, one can make narrower the frequency band, but the speed of scanning will be suppressed in the last case. When the "electro-magnetic" situation is more or less stable and all the signals are issued by continuous-wave sources, the probability of finding the desirable signal is rather high. However, sources of signals are, let say, "exotic" and give, for example, jumps in frequency domain, the probability of finding a pre-scripted source will be decreasing very fast. To grow the probability of finding the processing can be organized in a parallel manner with the needed number of narrow-band filters, see Fig.4.1. Similar systems had been called as panoramic receivers due to their parallelism providing a simultaneous parallel operation with really large number of such filters. The outputs of these filters are connected with square-law detectors, so that the output signals from detectors are directly proportional to the input signal power at each individual frequency of analysis. After that, this power is integrated within the time interval correlated with bandwidth of the corresponding filter. Technical problems of realizing for similar system include at least two factors. At first, the central frequencies are strongly individual in each frequency channel of processing; consequently, each filter has to be produced individually. Then, if now the radio-wave signal belongs to an ultra-high-frequency range, the design of filters became too complicated, so that the system as a whole will require large energy consumption and will be rather cumbersome.

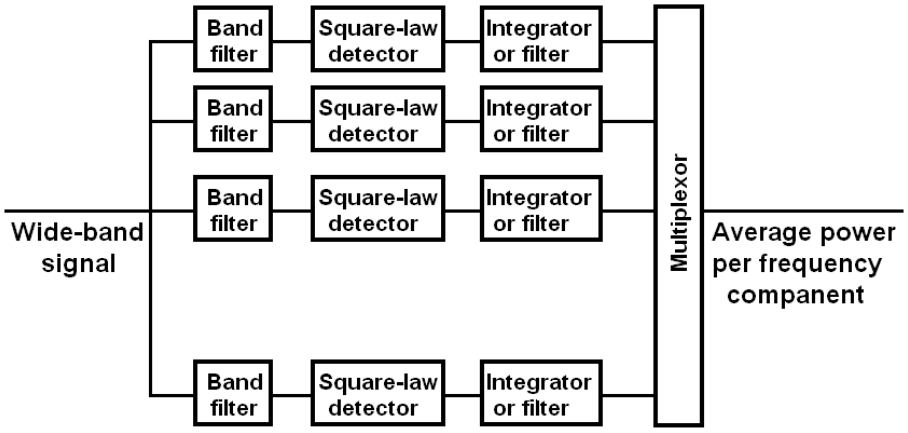

Figure 4.1. Structural scheme for the parallel electronic spectrum analyzer.

Finally, one can consider a typical acousto-optical spectrum analyzer, see Fig.4.2. these systems had been realized with, for example, two options, looking as the extreme options: on the one hand side, the frequency bandwidth is about **50 MHz**, the processing time is about **30 μs**, and the number of parallel channels **2000**, while on the other hand side, the frequency bandwidth is about **1.0 GHz**, the processing time is about **1.0 μs**, and the number of parallel channels **1000**.

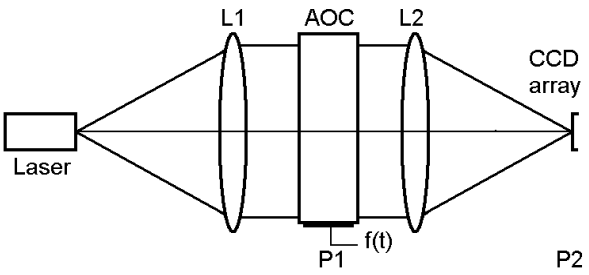

Figure 4.2. Optical layout from structural scheme for the acousto-optic spectrum analyzer.

Performance data inherent in the majority of similar systems lee usually between these extreme cases with more or less the same time-bandwidth product $\mathbf{1000-1500}$. Acousto-optical spectrum analyzer includes the laser source of monochromatic light, which is directed to the AOC through the lens $\mathbf{L1}$ or another collimating optics in such a way that the needed angular requirements are satisfied. In its turn, the AOC is excited by a wide-frequency signal correlated with those angular requirements. The integrating lens $\mathbf{L2}$ converts the angular spectrum into the linear one and focuses plane waves in an amount of spots lying in its focal plane. The photo-detector is represented by a multi-pixel CCD-linear array, which shapes a discrete video-signal. The number of pixels exceeds usually the time-bandwidth product by $\mathbf{2-3}$ times to provide the needed discreteness of a spectrum under analysis. Due to each doublet or maybe triplet of pixels is equivalent to a single frequency channel, the CCD-linear arrays have usually from 1024 to 4096 pixels, and the expected number of frequency channels can be really large, the advantages of acousto-optical spectrum analyzers can be easily estimated. Natural parallelism inherent in the optical system illustrates potential superiority of the acousto-optics in comparison with electronics in this area.

During the operation of acousto-optical spectrum analyzer lighting the AOC is realized almost perpendicular to its input optical facet, and together with this the piezoelectric transducer of that AOPC is exited by an external electronic signal $\mathbf{f(t)}$, so that the light wave signal at the output facet can be finally represented as $\mathbf{f(z,t)}$. The lens $\mathbf{L2}$ realizes the Fourier transform $\mathbf{F(w,t)}$ in the plane $\mathbf{P2}$, where

$$\mathbf{F(w,t)=\int_{-\infty}^{\infty} f(z,t)\cdot exp(2\pi i w z)\,dz}, \qquad (4.1)$$

where the space frequency $\mathbf{w}$ is connected with the physical coordinate ζ in the plane $\mathbf{P2}$ and the focal distance $\mathbf{F}$ of the integrating lens $\mathbf{L2}$ as $\mathbf{w=\zeta/(\lambda F)}$. In practice, the integration limits are limited by aperture of the AOC. Because of integration in Eq.(4.1) is performed with respect of the space coordinate at the input plane of a cell, one can say that this analyzed belongs to a group of architectures with the space integrating.

4.1.1. FREQUENCY RESOLUTION

The ability to resolve signals in frequency domain is oriented on fixing the gap of a pre-scripted depth between two frequencies in the Fourier domain. Moreover, the roots of similar ability are connected with the Rayleigh criterion for resolution within determining the angular distance

between stars using a telescope. The Rayleigh criterion is based on the uniformity of lighting the telescope aperture, so that light intensity in the image plane is described by the squared **sinc**-function. In so doing, the gap of a $\mathbf{1dB-}$depth can be obtained with a peak magnitude for the one frequency component coincides with the first zero for the neighboring frequency component. The gap of such a depth is well seen visually as well as on a photo-film. Applying the Rayleigh criterion to the acousto-optical spectrum analyzer, one can find that spatial distance $\delta\zeta$ between two neighboring frequency component in the focal plane of the integrating lens $\mathbf{L2}$ can be estimated as $\delta\zeta = \lambda F/D = \delta f \cdot \lambda FV$, where $\mathbf{F}$ is the focal distance of the lens $\mathbf{L2}$, $\mathbf{D}$ is the aperture of the AOC, $\mathbf{V}$ is the acoustic velocity, and $\delta\mathbf{f}$ is the frequency resolution. These equalities give us $\delta f = V/D = 1/(transittime)$. If one needs to require $\mathbf{2-3\,dB}$ depth of that gap, the frequency resolution will be reasonably changed. Moreover, one can apply various techniques for the incident light apodization to detect definitely weak signals. However, the suppressing of side lobes can be achieved by the expense of the corresponding demerit in the frequency resolution.

4.1.2. SPUR-FREE DYNAMIC RANGE AND INTERMODULATIONS

Potential nonlinearity of the transfer function peculiar to the AOC leads to appearing harmonic distortions and parasitic frequency components inside the frequency band. The level of these intermodulations is characterized by the spur-free dynamic range (SFDR), which can be determined as a ratio of the light intensity related to intermodulations to the intensity of a signal at the true frequencies, as it is shown in Fig.4.3 for a three-tone case. To protect a given SFDR, usually one has to restrict the diffraction efficiency of light scattering for each individual frequency component in a signal by the value $\chi_f \approx 3 \cdot \sqrt{SFDR}$.

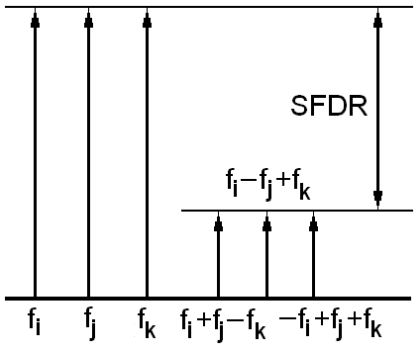

Figure 4.3. Illustration for the spur-free dynamic range (SFDR).

Thus, if, for instance, the SFDR about $\mathbf{50dB}$ is needed, one can find that $\chi_f \le 0.009$, which is close enough to approximately $\mathbf{1\%-}$ efficiency for an individual frequency component.

4.2. SPECTRUM ANALYZER WITH THE TIME INTEGRATION

The chirp $\mathbf{Z-}$transform is a method, which is often exploited for performing the Fourier transform in systems where only the time variable is known. The chirp $\mathbf{Z-}$transform is based on the fact that

the factor $2\pi\zeta z/(\lambda F)$ in the kernel of Fourier transform is equal to $\pi[\zeta^2+z^2-(\zeta-z)^2/(\lambda F)]$. The equivalent way for explaining the Fourier-transform determined by Eq.(4.1) gives

$$F(w,t)=\exp[\pi i\zeta^2/(\lambda F)]\cdot\int_{-\infty}^{\infty}\{f(z,t)\cdot\exp[\pi i z^2/(\lambda F)]\}\cdot\exp[-\pi i(\zeta-z)^2/(\lambda F)]\,dz. \quad (4.2)$$

This formula demonstrates that at first the optical signal $f(z,t)$ at the output facet is multiplied by the factor $\exp[\pi i z^2/(\lambda F)]$. Then, the Fresnel transform of the obtained product is fulfilled, and finally the result of integration is multiplied by the factor $\exp[\pi i\zeta^2/(\lambda F)]$ to compensate a square-law phase factor. The Fresnel transform in optics means that a light beam with some space distribution is propagating at a distance F in free space; in principle, it is a physical phenomenon accompanied by a dispersion when the angle of light dispersion is linearly depending on both time and space frequencies at the input. Figure 4.4 represents a configuration for an optical system capable of the chirp $Z-$transform, and one can see its analogy with the Fourier-transform system depicted in Fig.4.2; their difference consist in only positions of lenses. The lens $L1$ lights an external electronic signal $f(t)$ by coherent light beam, providing its pre-multiplication by the factor $\exp[\pi i z^2/(\lambda F)]$. The resulting beam propagation in free space realizes the operation of integral convolution, while the lens $L2$ gives us the needed post-multiplication.

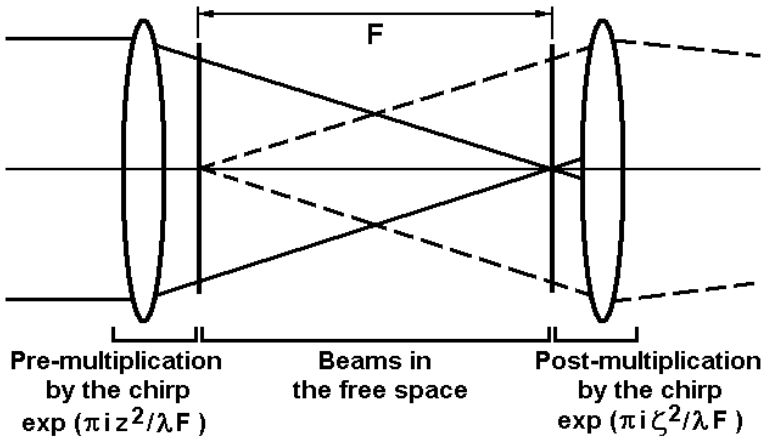

Figure 4.4. Optical scheme for the chirp $Z-$transform.

Application of the chirp $Z-$transform to various system architectures provides their significant flexibility relative to both the frequency resolution and the frequency bandwidth for analysis and makes it possible to design spectrum analyzers with the time integration, which have considerably improved frequency resolution.

If, for instance, one has a three input-port architecture with the point light source and a pair of the AOCs, both the AOCs should be mapped on the image plane. In this case, the first AOC has to be exited by the chirped signal $\cos(\pi at^2)$ during the time interval kT, while the second AOC has to be exited by the same-chirped signal $\cos(\pi at^2)$ in such a way that acoustic wave is passing in opposite direction through the second cell. Together with this, the point light source is electronically

modulated by a time-dependent signal $s(t)$, whose spectrum should be analyzed. In this case, light intensity in the image plane includes, in particular, the following combinational term

$$g_3(u) = \cos(2\pi f_S u/V) \int_0^{kT} s(t) \cdot \exp(\pi i a t u/V)\, dt, \qquad (4.3)$$

where non-significant constants are omitted. One can see that Eq.(4.3) represents the desirable Fourier transform of a time-dependent signal $s(t)$ with an arbitrary time interval kT of integration. Just this fact exhibits a reason, which provides approximately the $k-$times higher frequency resolution in a regime of the time integration in comparison with the spectrum analyzer based on the space integration. The presence of the space carrier frequency $\cos(2\pi f_S u/V)$ gives the reliable opportunity to separate the desirable combinational term $g_3(u)$ from the other signals in a system.

Here the frequency variable has the mathematical form $v = 2\pi wu/V$, and the bandwidth for analysis is $\Delta V = wT$. Due to the number of resolvable spots is $N = T \cdot \Delta f$, a new magnitude of the bandwidth for analysis will be determined by $\Delta V = \Delta f/k$. One can obviously see that both values v and ΔV depend on the velocity of frequency variation a within the frequency chirp. Therefore, the bandwidth for analysis as well as the frequency resolution can be varied electronically controlling the velocity of frequency variation a within the frequency chirp and the factor k of time integrating. It is seen that grows of the factor k in a view of increasing the frequency resolution δf leads to decreasing a new magnitude of the frequency bandwidth ΔV.

Let us consider a numerical example and suppose that one has the AOC with the frequency bandwidth $100\,MHz$ and the transit time about $10\,\mu s$, so that the time-bandwidth product is about $T \cdot \Delta f = 1000$. Using this AOC in the architecture with the space integration, one could realize $\delta f = 100\,kHz$ in the frequency bandwidth $\Delta f = 100\,MHz$. If now one need create the spectrum analyzer with the time integration providing the frequency resolution $\delta f = 1\,kHz$, one can request the time integrating factor as $k = (1\,ms)/(10\,\mu s) = 100$. The overlapping frequency range now is narrowed down to $\Delta V = 1\,MHz$, while the velocity of frequency variation within the frequency chirp, which will be in need to achieve the required time of integration, is characterized by the magnitude $a = 10^{11}\,GHz/s$.

5. MOTIVATION: GENERAL SCHEME FOR THE SPACE-AND-TIME-INTEGRATING SPECTRUM ANALYZER

It is well known that two-dimensional input devices can operate with patterns consisting of about 10^6 resolvable spots, while the time-bandwidth product of one-dimensional input devices cannot exceed about $10^3 - 10^4$. In principle, this difficulty can be resolved through the division of calculations on sequentional intermediate stages, associated with performances of one-dimensional input devices, and the exploitation of an external electronic memory for collecting intermediate data and assembling the final results. Such an approach is quite realistic, but it could give the lost of all the advantages peculiar to optical data processing. An alternative approach can eliminate involving an external electronic memory due to the use of specific photo-detector as a device for both memorizing intermediate data and producing the final results. In more details, intermediate data of calculations can be obtained exploiting the space-integrating in optical system, while collecting intermediate data and shaping the final results can be provided via time-integrating by the CCD matrix photo-detector. By this it means that one spatial variable and time create a two-dimensional space, wherein the initial pattern can be represented and processed on the basis of the space-and-time-integrating algorithm. Thus, the goal for designing the time-and space-integrating processor is connected with the possibility of replacing two-dimensional input devices by one-dimensional ones.

The technique of signal processing based on the space-and-time-integrating had been proposed for the spectrum analysis of one-dimensional signals [5.1, 5.2]. In principle, the analysis of one-dimensional signals can be provided by one-dimensional acousto-optical analyzer with only the space- or only the time-integrating. However, these analyzers have the performances supplementing with one another. The space-integrating gives a wide frequency bandwidth together with relatively low frequency resolution, while the time-integrating provides a high resolution for spectrum components accompanied by comparably narrow frequency bandwidth. A two-dimensional processor combining the advantages from both space- and time- integrating makes it possible to obtain the analysis with wide bandwidth as well as with high resolution simultaneously. A scheme of the space-and-time integrating spectrum analyzer exploiting a pair of the acousto-optical cells (AOCs) is shown in Fig.5.1. The triple product acousto-optical processor under design is intended for investigations in the extra-galactic astronomy as well as for exploring the extra-solar planets, which both need the algorithm of the space-and-time integrating providing rather wideband studies with an uprated spectral resolution. This processor includes a pair of mutually orthogonally oriented wide-aperture $1D$-acousto-optic cells as the input devices for a $2D$-optical spectrum analysis. Significance of this approach is conditioned by the usage of so-called chirp $Z-$ transform technique realizing a $2D$-Fourier transform of the input signal $s(t)$. That technique involves two frequency-chirp signals whose parameters $k_x x/(2\pi V)$ and $k_y y/(2\pi V)$ represent the frequency variables along the output axes x and y (V is the acoustic velocity). If the factor k_x is chosen so that $k_x D/(2\pi V) = \Delta f$ is the bandwidth of the signal $s(t)$, the spectrum of $s(t)$ will be registered and shown along the axis x with relatively low resolution similar to the conventional space-integrating spectrum analysis. Its resolution is characterized by the value $\Delta f / M$ inherent in the performances of a $M \times M$-pixel CCD-matrix.

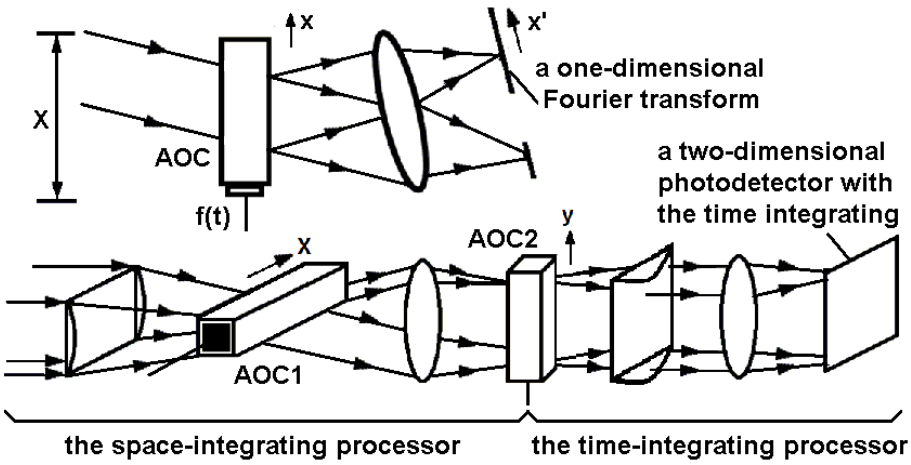

Figure 5.1. Spectrum analyzer with the space-and-time integrating [5.3].

If the time function $\mathbf{f(t)}$ is applied to the AOC as a signal, in the output focal plane of the last integrating lens, which produces the Fourier transform at a focal distance $\mathbf{F}$, one can find a distribution of light amplitudes modulated by the function

$$\mathbf{g(u,t)=\int_X f(t-x/V)\cdot exp(2\pi iux)\,dx=\{F(uV)\otimes sinc(XuV)\}\cdot exp(2\pi iVux)} \qquad (5.1)$$

where $\mathbf{X}$ is the linear size of optical aperture inherent in the AOC, $\mathbf{u=x_1/(\lambda F)}$ is the spatial frequency, $\mathbf{x_1}$ is the spatial coordinate in the output focal plane of the last integrating lens, and the sign $\otimes$ means the convolution. It is seen that spatial modulation of light in the output focal plane corresponds to a Fourier transform $\mathbf{F(uV)}$ of the time function $\mathbf{f(t)}$, smoothed due to its convolution with the function $\mathbf{sinc(XuV)}$ or $\mathbf{(sinx)/x}$ conditioned by a finite size of the AOC's optical aperture. As a result, the frequency resolution is determined by a width of the main lobe of $\mathbf{(sinx)/x}$, which is equal to $\mathbf{(V/x)}$ Hz. Together with this, the light amplitude at the output has sinusoidal time modulation as well at each point in spatial-frequency plane. Moreover, the frequency of time modulation is directly proportional to the spatial frequency $\mathbf{u}$. Taking into account all the light components, which are incidencing at a resolvable spot n the spatial frequency domain (with the space-frequency width $\mathbf{\lambda F/X}$), the spectrum width of the time modulation of light is equal only to $\mathbf{(V/X)}$, i.e. to the frequency resolution of space-integrating processor. Consequently, this time-modulated light beam can be used as the input signal for the time-integrating processor, operating within the chirp $\mathbf{Z-}$transform algorithm along an orthogonal direction, see Fig.5.1. In so doing, one can have shaped a spectrum of a narrow-band time signal with a high resolution in the points located inside each individual resolvable spot of the space-integrating processor. Together with this, all partial resolvable spots identified with a low resolution can be simultaneously processed by multi-channel time-integrating processor described above, see Fig.5.2. The bandwidth within time modulation of light in the frames of each individual resolvable spot related to spatial frequency is quantitatively equal to $\mathbf{(v/X)}$, but the central frequency of time modulation in each position is equal to $\mathbf{(nV/X)}$, where $\mathbf{n}$ is a whole number, which grows proportionally to particular location of a resolvable spot of the space-integrating processor. The

signals from all the frequency resolvable spots should be converted at video-frequencies before than they will be simultaneously processed by multi-channel time-integrating processor.

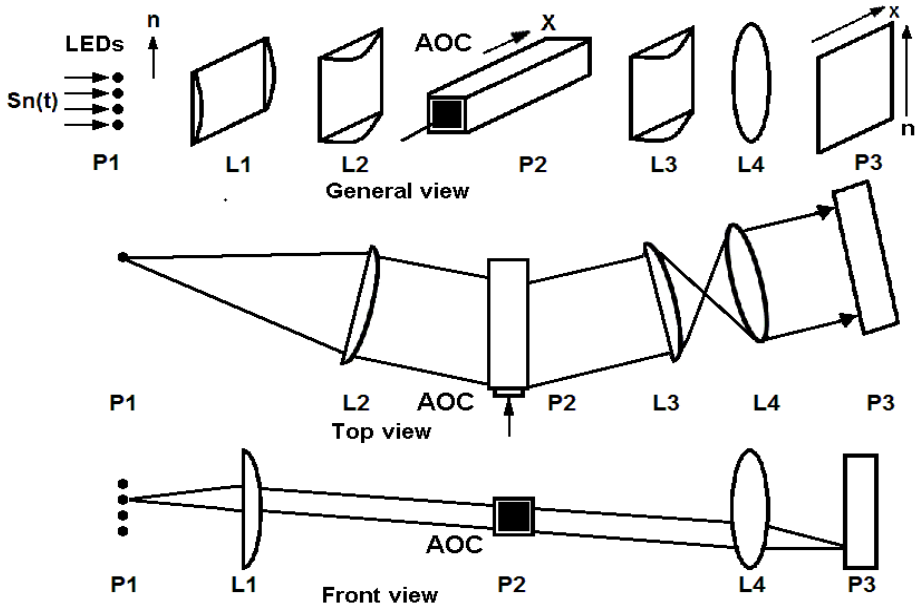

Figure 5.2. Multi-channel spectrum analyzer with the time-integrating [5.3].

To fulfill this requirement one can use a pulsed light source with the pulse repetition frequency (V/X). When individual pulses are short enough, the time modulation of light source can be approximated by a sum of the Dirac delta functions

$$\sum_{m}\delta[t-m(X/V)] \sim (V/X)\sum_{m}\exp[(imV/X)t] . \qquad (5.2)$$

At the output of space-integrating system, the light amplitude is modulated by a product of functions described by Eqs.(5.1) and (5.2). Then, Eq.(5.2) shows that periodic pulse sequence of light words includes all harmonic components of the main time frequency (v/X). This is why the modulating function with the central frequency (nv/X) will be mixed with the $n-th$ harmonic of a signal from the source of radiation on the $n-th$ element of resolution, so that as a result video-signals will be shaped on a photo-detector. Due to similar process takes place with all the values of n, these video-signals will be produced for each individual element of resolution as well. Thus, a multi-channel processor with the time-integrating realizes the Fourier transform with a high resolution relative the obtained video-signals within each channel and averages (down to the zero level) all high-frequency components. Finally, the folded spectrum of the signal $f(t)$ is formed at the output two-dimensional matrix of photo-detectors in a system with the time-integrating.

6. BRIEF DESCRIPTION OF POTENTIAL ADVANTAGES PECULIAR TO THE SPACE-AND-TIME INTEGRATING PROCESSOR

Let us apply the algorithm of so-called chirp–**Z**–transform technique to the signal $\mathbf{s(t)}$. In so doing, one can take, for example: $\mathbf{V = V_1 = V_2}$, $\mathbf{\Phi_0(t) = s(t)\cdot exp(ik_1 t^2 + ik_2 t^2)}$, $\mathbf{\Phi_1(t) = exp(-ik_1 t^2)}$, and $\mathbf{\Phi_2(t) = exp(-ik_2 t^2)}$. As a result the output function will have the form:

$$\mathbf{g(x,y) = exp[-ik_1 (x/V)^2 - ik_2 (y/V)^2] \times \int_{T_i} s(t)\cdot exp[-2ik_1 (x/V)t - 2ik_2 (y/V)t]\, dt}\,. \quad (6.1)$$

Without the square-law phase term, the function $\mathbf{g(x,y)}$ can be considered as the Fourier-transform of the signal $\mathbf{s(t)}$, which has been calculated using the algorithm of chirp–**Z**–transform with respect to both the space coordinates. The values $\mathbf{k_1 x/(2\pi V)}$ and $\mathbf{k_2 x/(2\pi V)}$ manifest themselves as the frequency variables along the axes $\mathbf{x}$ and $\mathbf{y}$, respectively, so that spectrum of the signal $\mathbf{s(t)}$ will be displayed along the coordinates $\mathbf{x}$ and $\mathbf{y}$. Maximal frequencies for the spectrum inherent in the signal $\mathbf{s(t)}$ and presented along the axes $\mathbf{x}$ and $\mathbf{y}$ are equal to $\mathbf{k_1 D/(2\pi V)}$ and $\mathbf{k_2 D/(2\pi V)}$, where $\mathbf{D}$ is the apertures of both the AOCs. If the factor $\mathbf{k_1}$ is chosen in such a way that $\mathbf{k_1 D/(2\pi V) = \Delta f}$ for the signal $\mathbf{s(t)}$, the complete frequency spectrum of this signal will be represented along the axis $\mathbf{x}$ with relatively low frequency resolution corresponding to the conventional space-integrating spectrum analysis. This estimation is conditioned by the fact that resolution is determined by the ratio of the frequency bandwidth $\mathbf{\Delta f}$ to the number $\mathbf{M}$ of pixels peculiar to the taken $\mathbf{M \times M}$ CCD-matrix along the axis $\mathbf{x}$, i.e. the frequency resolution is characterized by the value $\mathbf{\Delta f / M}$. If together with this the factor $\mathbf{k_2}$ is selected as $\mathbf{k_1 / M}$, one has arrived at the case when only a $\mathbf{1/M}$-part of a spectrum will be depicted along the axis $\mathbf{y}$ for each individual position along the axis $\mathbf{x}$. As a result, the frequency resolution along the axis $\mathbf{y}$ becomes to be equal to the value $\mathbf{\Delta f / M^2}$. These estimations are true under condition that the time of integration $\mathbf{T_i}$ exceeds $\mathbf{M^2 / \Delta f}$. By the way, such a combination of the transformation along the axis $\mathbf{x}$ with relatively low resolution in a wide frequency bandwidth with the transformation along the axis $\mathbf{y}$ with a high frequency resolution, but in a narrow frequency bandwidth represents a two-dimensional folded spectrum or a two-dimensional raster for recording $\mathbf{M^2}$ counts of one-dimensional Fourier-images of the signal $\mathbf{s(t)}$. Shaping a one-dimensional spectrum along a pair of space coordinates within this architecture makes it possible to display up to $\mathbf{M^2}$ spectrum components, because the matrix of photo-detectors has just $\mathbf{M^2}$ pixels. Thus, this technique provides potentially a high frequency resolution together with rather wide frequency bandwidth of the spectrum analysis. Finally, this processor produces the resultant folded spectrum, which is subject to electronic post-processing. Generally, this technique accumulates principal advantages of both space and time integrating acousto-optical processors. In particular, with the typical value $\mathbf{M = 10^3}$ similar system exhibits rather wide frequency bandwidth $\mathbf{\Delta f}$, which is practically equal to

bandwidth of the input piezoelectric transducers of acousto-optical cells. The magnitude of Δf can be estimated from $30\,MHz$ to about $1\,GHz$. Together with this similar system is able to provide a high frequency resolution δf, which is practically equal to the reciprocal of the CCD-matrix photo-detector integration time $1/T_i$. Within optimal choosing of both the integration time T_i and the above-noted factors $k_{1,2}$ inherent in a pair of the frequency-chirp signals, one can vary the needed frequency resolution δf from about $10\,Hz$ to $10\,KHz$.

7. GENERAL SCHEMATIC ARRANGEMENT AND CURRENT DESIGN

One of the allowable practical realizations of the above-characterized optical scheme for the triple-product acousto-optical processor, i.e. for a spectrum analyzer with the space-and-time integrating, depicted in Fig.5.1, is presented as a simplified prototype in Figs.7.1 and 7.2.

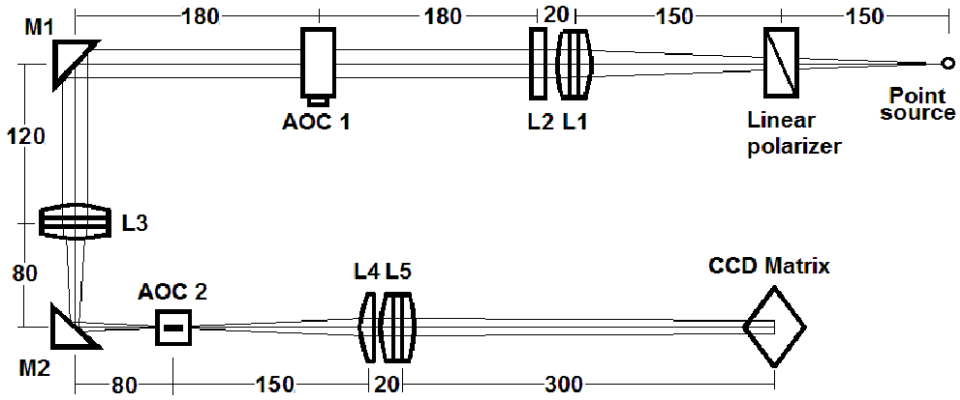

Figure 7.1. Layout of the simplified optical scheme for the acousto-optical triple-product processor.

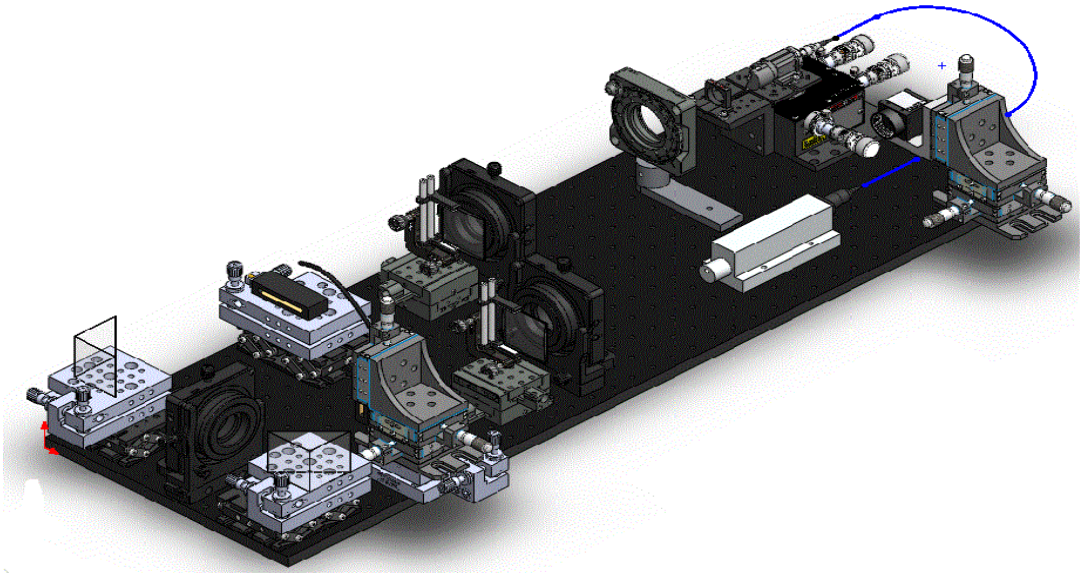

Figure 7.2. Potential simplified design of a prototype for the triple-product acousto-optical processor.

The designed arrangement is localized on a $3\times1-$ feet optical breadboard and based on specifically selected and optimized set of two-inch spherical and cylindrical lenses. The solid-state laser, allowing an external amplitude modulation with the frequency up to $250\,MHz$ can be potentially chosen as a point source of light due to its light output is arranged through a connector with a span of the single mode optical fiber.

8. PRELIMINARY CHARACTERIZATION OF SELECTED POTENTIAL COMPONENTS

The selected optical and mechanical components make it possible to use of highly effective and specially designed wide-aperture AOCs. For this purpose, in particular, one can consider such spatially one-channel tellurium dioxide (TeO_2) crystalline AOC as the cell TED.30–75–50–633 (Brimrose Corp.). It has the transit time $T \approx 30\,\mu s$, the optical aperture $3 \times 21\,mm$, the frequency bandwidth $50\,MHz$ at the carrier frequency $75\,MHz$, so that the time-bandwidth product is about 1500, see Table 8.1. The AOC based on TeO_2 -crystal (Brimrose Corp.) is presented in Fig.8.3.

Time-bandwidth product	1500
Center frequency	75 MHz
3 dB Bandwidth	50 MHz
Access time or aperture	30 μs / 3x21mm
Deflection angle	3 deg.
Diffraction efficiency	> 65 %
Acoustic velocity	660 m/s
Wavelength	633 nm

Table 8.1. Parameters of the AOC . TED.30–75–50–633

Figure 8.3. A TeO_2 -crystal based AOC (Brimrose Corp.).

The CCD matrix camera **DCU224** (Thorlabs) can be potentially considered as the time-integrating multi-pixel (more than 10^6 **pixels**) photo-detector due to its high dynamic range, which allows imaging a wide range of light intensities. This camera is presented in Fig.8.4, while its performances are illustrated by Table 8.2.

Figure 8.4. The CCD matrix **.** Thorlabs **DCU224C**

Sensor type	CCD
Resolution	1280 x 1024
Optical sensor class	1/2“
Sensitive area	5.95 x 4.76 mm²
Pixel size	4.65 μm
Frame rate	15 fps
Exposure time	83 μs -1460 ms
Interface	USB 2.0
Temperature	0 - 50° C
Pixel size	4.65 x 4.65 μm²

Table 8.2. Parameters of the CCD matrix shown in Fig.8.4.

8.1. LENS CHARACTERIZATION

8.1.1. SURFACE FLATNESS

Often the design of an optical system requires evaluation of the intensity in the diffraction pattern near the Gaussian focus. This is a very difficult and tedious calculation when aberrations must be considered. Previously, Born and Wolf [8.1] have reported analytical results for the three-dimensional diffraction pattern near the Gaussian focus associated with each individual primary aberration, but to obtain an analytical result for a perfectly general aberration would be hopelessly lengthy. Another possible approach is to avoid the analytical methods and evaluate the wave front distortion with standard ray-tracing techniques and then ingress the Fraunhoffer diffraction integral by employing numerical methods with the aid of a computer. Later, other one had found that the beam intensity at the Gaussian image point is not seriously degraded by other primary aberrations if the maximum wave front deviation remained less than a quarter wavelength. This result became known as Rayleigh's quarter wavelength rule. Maréchal further developed the idea of relating the intensity degradation at the Gaussian image to the wave front distortion. By assuming a uniformly illuminated aperture, he was able to calculate the ratio of the peak far-field intensity for a system with aberrations of the same system without aberration. This ratio can be defined as $\mathbf{j}$, so that the Maréchal's result takes the form

$$\mathbf{j} = \mathbf{1} - \left(\frac{2\pi}{\lambda}\right)^2 (\Delta\Phi)^2 \ . \tag{8.1}$$

Here, λ is the light wavelength and $(\Delta\Phi)^2$ is the mean square deviation of the wave front from the reference sphere. Actually, this result for $\mathbf{j}$ is an approximate evaluation of the Strehl definition, valid for small aberrations, but one shall refer to it as the intensity degradation, or the Maréchal intensity criterion. As a comparison with the Rayleigh quarter-wavelength rule, one can find that for $|(\Delta\Phi)^2| \leq \lambda/\mathbf{14}$ a degradation less than $\mathbf{20\%}$. Equation (8.1) permits us to calculate directly the relative peak intensity in the far-field diffraction pattern if the wave front deformation is not too severe, to set tolerances on the individual surface errors, and to determine which surface or aberration is the primary contributor to the intensity degradation. The current software in optics, such as Zemax and OSLO, use the measurement in the root-mean-square value of the flatness. This technique involves measuring a substantial amount of the optic's surface at many points and then calculating the standard deviation of the surface from an ideal form. Similar measurement has direct mathematical implications: for instance, it is possible to calculate the Strehl ratio from it. Practically, the Strehl ratio is a very good indication on how much power one gets at the image plane of the optical system versus what power one will get from an ideal aberration-free system.
Once the Strehl ratio has been calculated, the quality of the optical system may be ascertained using the Maréchal criterion. The Maréchal criterion states that a system is regarded as well corrected if the Strehl ratio is greater than or equal to $\mathbf{0.8}$, which corresponds to a root-mean-square wave front error $\lambda/\mathbf{14}$. For example, an optical system introducing a $\lambda/\mathbf{3}$ root-mean-square deformation will have his actual power at focus reduced to approximately $\mathbf{3\%}$ of its theoretical power. The reason for this drop in power at the focus is that some interferences are created in the focus with different rays arriving with a different phase.

The point-spread function (PSF) is a functional form identical to that of the image generated by $\delta-$ pulse input. It's the impulse response of the system whether optically perfect or not. In a well-corrected system, the PSF is the Airy irradiance distribution function centered on the Gaussian image point (see later Fig.8.2). In addition to this, it is possible to estimate the theoretical Fraunhoffer diffraction pattern in a system without aberrations

$$\mathbf{I(\theta)=\left[\frac{2\,J_1\,(k\,a\cdot\sin\theta)}{k\,a\cdot\sin\theta}\right]^2}, \tag{8.2}$$

where $\mathbf{\sin\theta = r/z}$. One can write the intensity of the Fraunhoffer diffraction pattern for a circular aperture as

$$\mathbf{I(r)=\left(\frac{A}{\lambda\,z}\right)^2\left[2\,\frac{J_1(k\,\omega\,r/z)}{(k\,\omega\,r/z)}\right]^2}, \tag{8.3}$$

where $\mathbf{A=\pi\omega^2}$; then, $\boldsymbol{\omega}$ is the radius of aperture, $\mathbf{r}$ is the radius coordinate in the observational plane, $\mathbf{k}$ is the wave number, $\mathbf{z}$ is the focal length, and $\mathbf{J_1}$ is the Bessel function. For a rectangular aperture the Fraunhoffer diffraction pattern is given, of course, by

$$\mathbf{I(x,y)=\left(\frac{A}{\lambda\,z}\right)^2\sin c^2\left(\frac{2\,\omega_x\,x}{\lambda\,z}\right)\sin c^2\left(\frac{2\,\omega_y\,y}{\lambda\,z}\right)}\ . \tag{8.4}$$

Rather often the term "diffraction limited" is used in practice. This term implies that the physical effects of light diffraction rather than imperfections in either the design or fabrication limit the performances of an optical system. There are many ways of determining an optical system as the "diffraction limited" one using such characteristics as, for example, the Strehl ratio, root-mean-square OPD, standard deviation, maximum slope error, and others. Nevertheless, it is possible for a system to be considered diffraction limited by one method and not diffraction limited by another method. In connection with the said before, the Maréchal criterion states that, if the Strehl ratio exceeds $\mathbf{0.8}$, a lens system may be described as the "diffraction limited" system.

In a view of the needed lens characterization, the comparison of various adequate spherical and cylindrical lenses from the most known manufactures of optical components has been carried out. To estimate the quality of each individual lens the software OSLO or/and Zemax, whose purpose is the synthesis, analysis, and optimization of lenses, have been exploited. With these programs, it is possible to choose a desirable lens in a given catalogue and to simulate their optical aberrations. They also allow us to estimate the Strehl ratio at a given light wavelength. For our purposes, the lenses of two inches in diameter for spherical lenses and two inches square for cylindrical lenses have been selected. The considered wavelength was $\mathbf{587\,nm}$ (the green-helium line). Performing the simulation with these programs made it possible to compare the diffraction pattern for both cylindrical and spherical lenses with the corresponding ideal theoretical lenses using Eqs.(8.3) or/and (8.4) as the case requires.

Now, let us consider some details of these estimations. Figure 8.1 shows the patterns of rays directing on the image plane form a single-point object in the case of using the "geometrical

approximation" which ignores the wave nature of light. The line represents the ray trace that collimate in a single point.

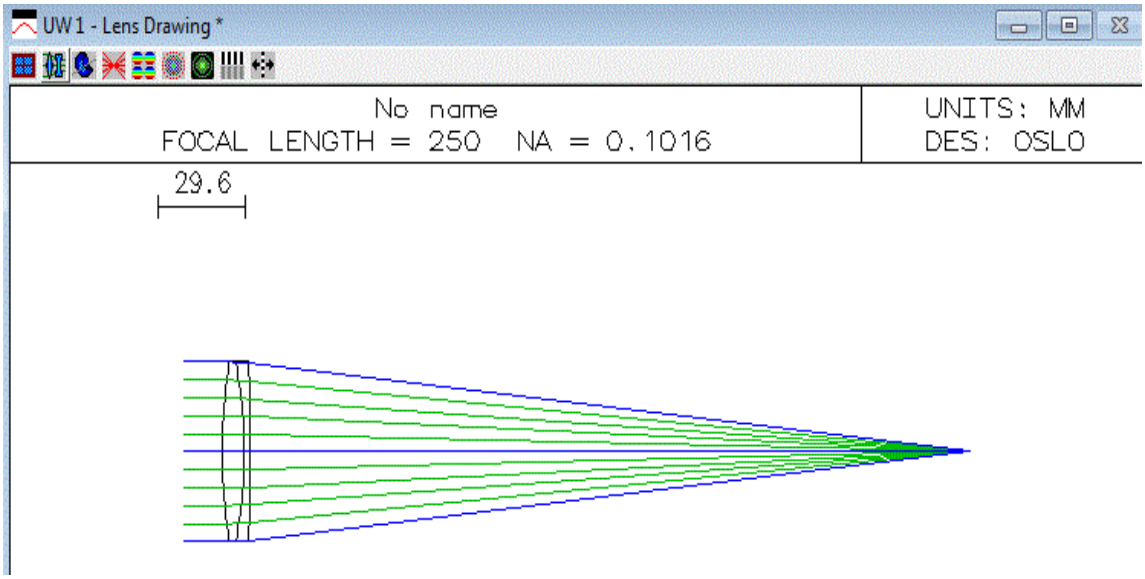

Figure 8.1. Ray traces of a cylindrical lens obtained with the software OSLO.

Figures 8.2 – 8.5 represent the PSF and demonstrate the profiles resulting irradiance distribution in the image plane. Figure 8.2 illustrates the optical scheme of theoretical behavior for the point spread function, when the light passes thought a lens, and then the distribution of the electric field intensity is produced by the effect of just far-field Fraunhoffer diffraction. Due to the presence of an axial symmetry, the central maximum corresponds to the circular nucleus of high irradiance dominated Airy disc; this fact is shown in Fig. 8.3.

Figure 8.4 depicts the distribution of light in the focal point. This picture is usually called the spot diagram. There are three shapes in the figure (triangular, square, and circle); each one represents an individual wavelength (blue, red, or green). A circle in the middle part corresponds to the first minimum of the Airy disc, which represents light intensity in the image of a perfect lens with the same aperture, but in monochromatic light at the central wavelength.

In Fig.8.5, the number of the scale on the right: **0.9949** is the Strehl ratio, the intensity at the central peak of the image of a point source normalized to that of the Airy diffraction pattern of an ideal lens. Its possible to see that at the Strehl ratio exceed **0.8** , one can assume that the lens exhibits the diffraction pattern.

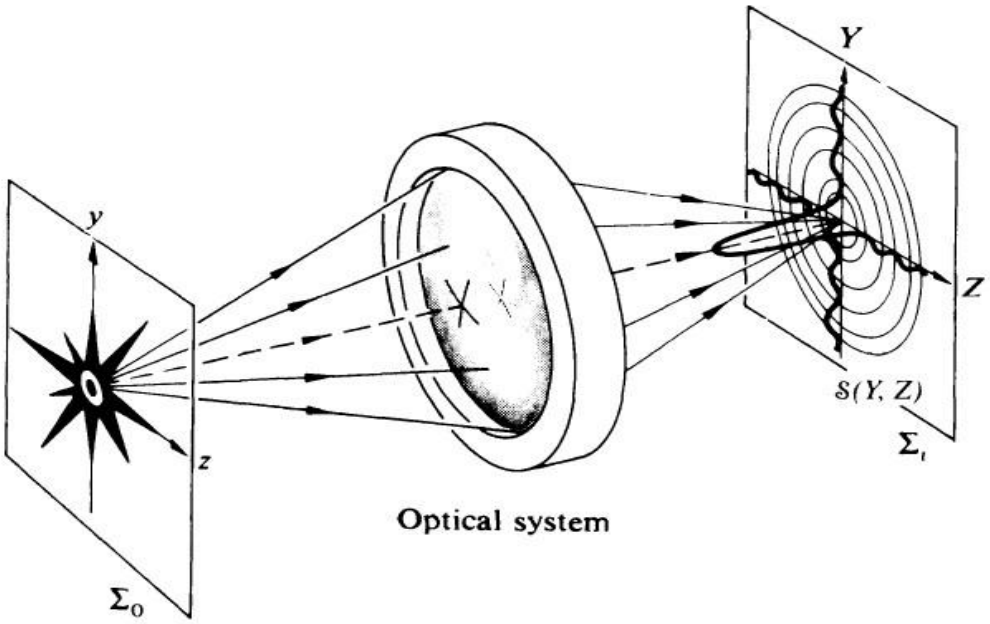

Figure 8.2. The point-spread function (PSF): the irradiance produced by the optical system with an input point source

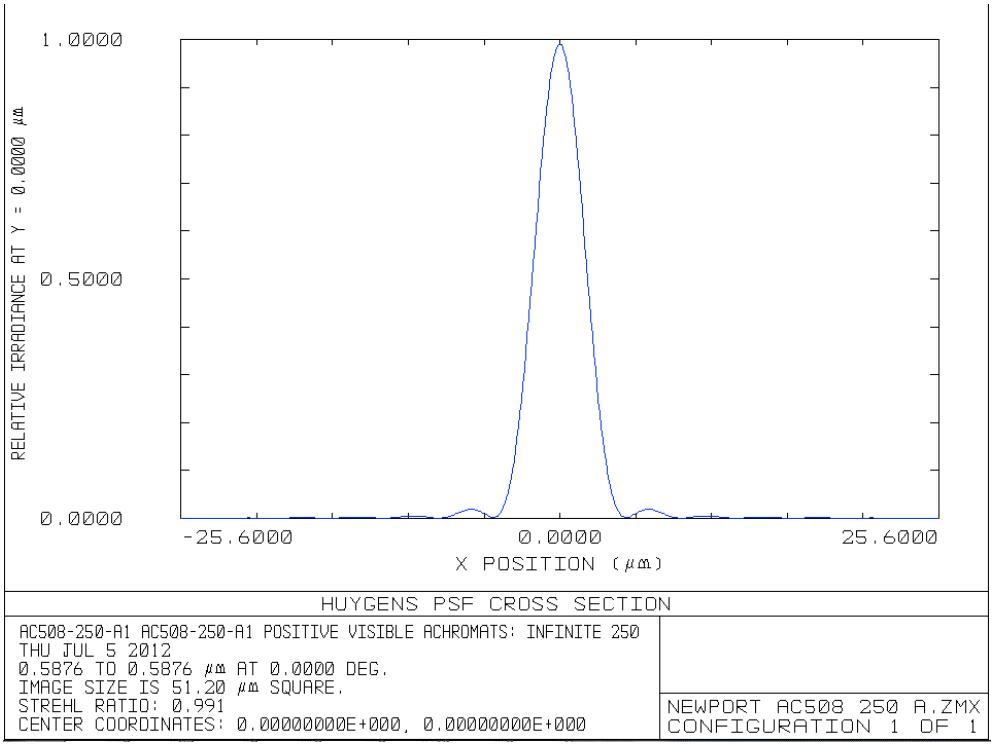

Figure 8.3. Point spread function (PSF) of a spherical lens, diameter of **50.8 mm**, focal length of **250 mm**.

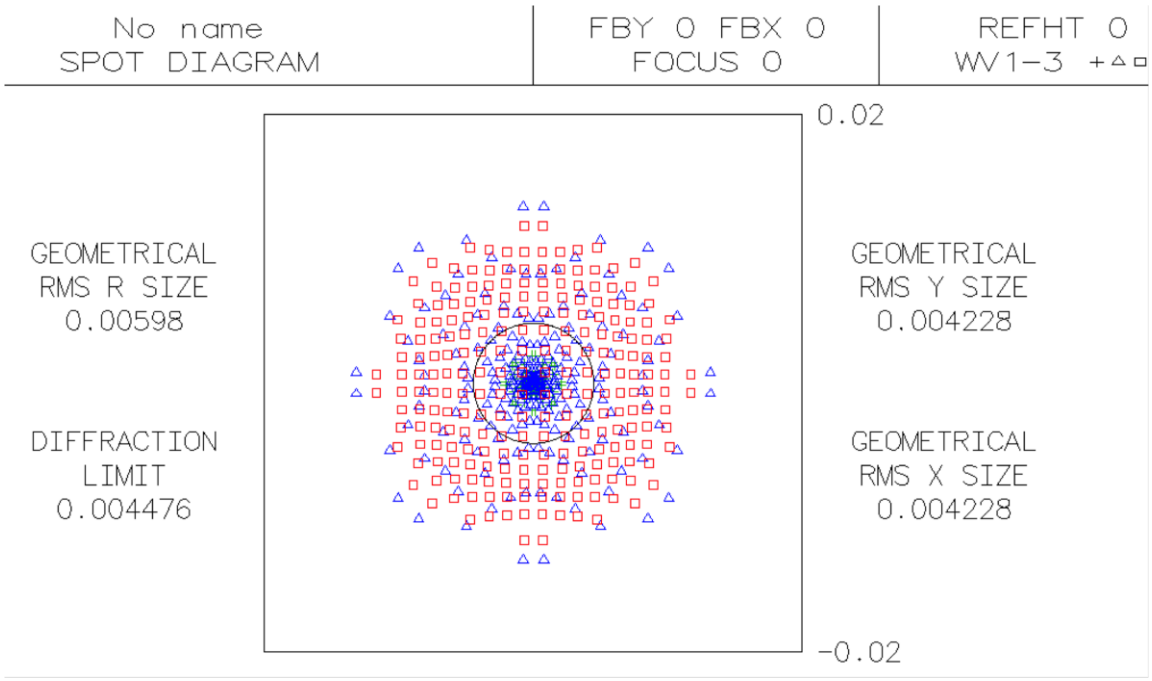

Figure 8.4. Spot diagram for a spherical lens with an aperture of **20 mm**, Diameter **50.8 mm**, focal length **250 mm** and central wavelength equal to **5876 nm**.

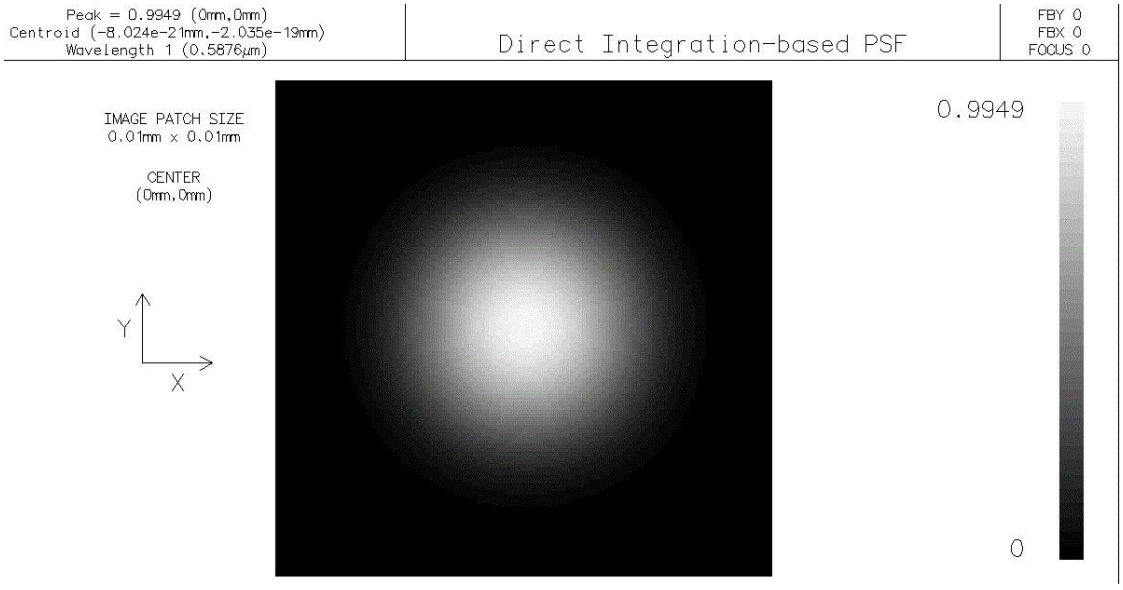

Figure 8.5. Point-spread function (PSF) reflecting the Strehl ratio equal to **0.9949** for the Thorlabs spherical lens

The following tables 8.1 – 8.3 give the Strehl ratio for various lenses from the catalogues of various companies. For all the cases the spherical lenses were considered for two inches in diameter and focal length varying in each table. Only the lenses, whose Strehl ratios are rather close to unity,

have been chosen for our analysis. The goal of this analysis consists in finding the best lenses for the system under design. Then, each table corresponds to an individual focal length.

Company	Lens	Strehl ratio, OSLO	Spot width	Strehl ratio,Zemax	Spot width
Thorlabs	AC508-250-A	0.9463	1.0567	0.991275	1.0088
Newport	PAC088	0.9899	1.01022	0.992112	1.0079
JML	DBL14170/100	0.9948	1.0052	0.928246	1.20737
Linos	G322311000	0.99436	1.00564	0.953530	1.048734

Table 8.1. Comparative table of different spherical lenses with the focal length $\mathbf{F = 250\,mm}$.

Company	Lens	Strehl ratio, OSLO	Spot width	Strehl ratio,Zemax	Spot width
Thorlabs	AC508-300-A	0.996326	1.03807	0.984867	1.015365
Newport	PAC089	0.990888	1.009195	0.820735	1.2184201
JML	DBL14195	0.994827	1.005189	0.915545	1.0922456
Ross	LAOC269	0.992602	1.007453	0.91386	1.094259

Table 8.2. Comparative table of different spherical lens with the focal length $\mathbf{F = 300\,mm}$.

Company	Lens	Strehl ratio, OSLO	Spot width	Strehl ratio,Zemax	Spot width
Thorlabs	AC508-500-A	0.994665	1.005363	0.984616	1.015624
Newport	PAC091	0.9971	1.00289	0.996042	1.003973
JML	DBL14235	0.99549	1.00451	0.998083	1.001921
Ross	LAOC271	0.99581	1.004192	0.998083	1.001921

Table 8.3. Comparative table of different spherical lens with the focal length $\mathbf{F = 500\,mm}$.

8.1.2. FINAL SELECTION OF THE LENSES

Finally for the above-chosen wavelength and two inches of diameter one had estimated the best lens for the above-mentioned tables and comparing with the theoretical estimations using Eqs.(8.2) and (8.3). The final selection of the lenses is as follow.

Company	Type	Part	Description	Quantity
Thorlabs	Spherical lens	AC508-250-A	D=2”, F=250mm	2
Thorlabs	Spherical lens	AC508-150-A	D=2”, F=150mm	1
Newport	Cylindrical lens	CKX300	50.8 x 50.8 mm, F = 300 mm	2
Newport	Right angle prism	BRP-50.8-A	50.8 mm	2
Newport	Linear polarizing glass filter	LPGF-2	D = 50mm, λ=400 - 700 nm	2

Table 8.4. The final selection of the components.

Figures 8.6 and 8.7 show the comparison between the diffraction patterns obtained theoretically with equations and simulated using OSLO curves, for both spherical and cylindrical lenses.

One can observe from Fig. 8.7 that the spherical lenses have good quality, i.e. really small optical arerrations, because the numerically simulated profiles for all the compared lenses are quite similar to the theoretical curves. By contrast with them, the cylindrical lenses have more aberrations; they

are very different from the theoretical plot, for example, within identifying the position of the first zero in light distribution.

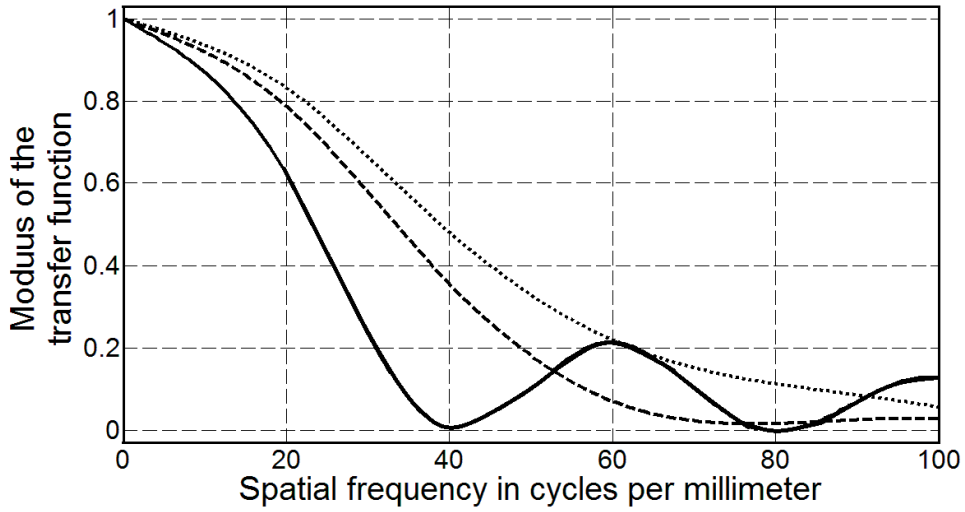

Figure 8.6. Comparison between the PSF and the Fraunhoffer diffraction pattern in the cylindrical lenses: the continuous line corresponds to the theoretical Fraunhoffer diffraction, while the dashed line is for the Thorlabs lens and the dotted line is for the Linos company lens.

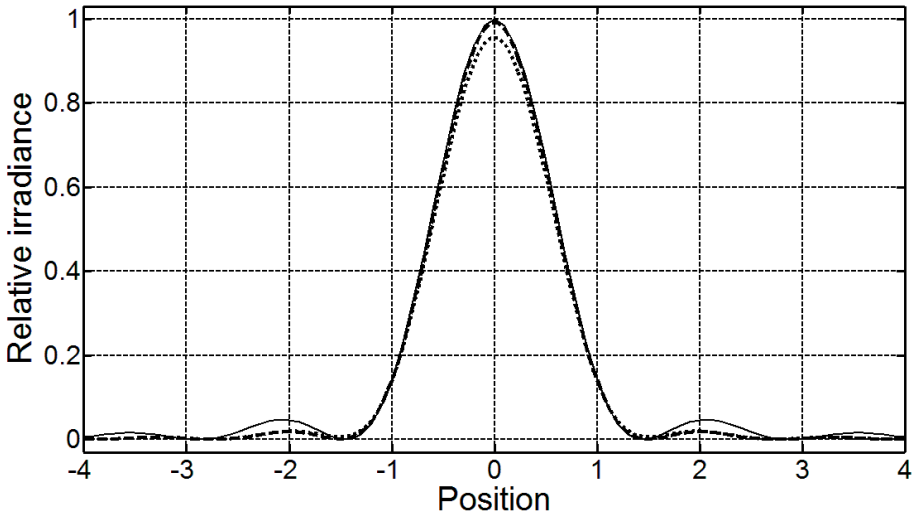

Figure 8.7. Comparison between the PSF and the Fraunhoffer diffraction pattern in the spherical lenses. The continuous line corresponds to the theoretical Fraunhoffer diffraction, while the dashed line is for the CVI Melles Griot lens, and the dotted line is for the Newport company lens.

9. REFERENCES

Section 2:

[2.1] P. Kellman. “Time integrating optical processing.” Ph. D. thesis. Stanford University (1979).

[2.2] T. M. Turpin. “Time integrating optical processing.” Proc. SPIE, vol.**154** (Real Time Signal Processing I); p.196 (1978).

Section 3:

[3.1] R. W. Klein and B. D. Cook. "A unified approach to ultrasonic light diffraction." IEEE Transactions of Sonics and Ultrasonics, vol. **SU-14**, no. 3, pp. 123-134 (1967).

Section 5:

[5.1] T. Bader. “Acousto-optic spectrum analysis. A high performance hybrid technique.” Appl. Optics, vol.18, p.1668 (1979).

[5.2] D. Psaltis and D. Casasent. “Time-and-space integrating spectrum analyzer.” Appl. Optics, vol.18, p.3203 (1979).

[5.3] A. Korpel. *Acousto-Optics.* (Marcel Dekker. New York. 1997).

Section 8:

[8.1] M. Born and E. Wolf. *Principles of Optics.* 7-th Ed. (Cambridge. 2009).

10. CONCLUSIVE REMARKS

The current state of designing the triple product acousto-optical processor in frames of the instrumentation for various astrophysical applications has been presented. The above-presented general consideration of a few key aspects related to creating an acousto-optical scheme of triple product processor reflects an indispensable step to practical design of similar processor. A reasonable part of this analysis is devoted to practical design of the schematic arrangement of this processor based currently on a two-inch optics and wide-aperture spatially one-channel AOCs made of the tellurium dioxide ($\mathbf{TeO_2}$) crystal. The layout of simplified optical scheme has been demonstrated, and general schematic arrangements of the triple-product acousto-optical processor as well as the principle characterizations for a few key components, such as the crystalline AOCs, specifically oriented CCD-matrix as well as specially selected and additionally estimated spherical and cylindrical lenses have been presented and briefly discussed.

11. ACKNOWLEDGMENT

This work has been financially supported by the CONACyT, Mexico within the projects # 61237 (initially) and # 15149 (currently).